ChemCatChem

Research Article
doi.org/10.1002/cctc.202300221

Chemistry Europe
European Chemical Societies Publishing

www.chemcatchem.org

Role of Titanium in Ti/SiO_2-Supported Metallocene-based Olefin Polymerization Catalysts. Part 1: Genesis of Active Sites and Catalytic Performance

Silvia Zanoni,[a] Alexandre Welle,[b] Virginie Cirriez,[b] and Bert M. Weckhuysen*[a]

Performance enhancement of metallocene-based olefin polymerization catalysts can be obtained, among others, by the chemical modification of their support. We investigated a titanated SiO_2 (Ti/SiO_2) as an improved support material for zirconocene catalysts, which lead to ~35% higher ethylene polymerization yields when compared to the unmodified SiO_2-supported metallocene. The improved catalytic performance of the modified catalyst was found to be related to the presence of a Ti-based active site, second to the Zirconocene centers, as well as to a higher Lewis acidity in the titanated supported-MAO, which improved the activation of the Zr-based centers. The Ti active species were generated by reduction of the Ti/SiO_2 support with the methylaluminoxane (MAO) co-catalysts, which introduced oxygen vacancies (V_O) and Ti^{3+} species, as confirmed by probe molecule Fourier Transform Infrared (FT-IR) spectroscopy and UV-Vis Diffuse Reflectance Spectroscopy (DRS). The higher Lewis acidity was linked to 5-coordinated Ti^{4+}, as detected by probe molecules FT-IR spectroscopy.

Introduction

Metallocene-based olefin polymerization catalysts consist of a group 4 transition metal center, typically Zr, coordinated to two cyclopentadienyl(-derivative) rings and two other ligands (halide or alkyl), Cp_2ZrL_2.[1] They can be activated toward the polymerization of olefins by a co-catalyst, such as methylaluminoxane (MAO).[2–6] The role of MAO is linked to its Lewis acidic character together with its terminal $AlMe_2^+$ and free trimethylaluminum (TMA) species, which together alkylate the transition metal (when in the halide form) and ionize it, leading to a metal-CH_3 site with a cationic vacancy $[Cp_2ZrMe]^+$. On this site, olefins can insert and polymerize via the Cossee-Arlman mechanism.[7–13] In addition, the MAO terminal $AlMe_2^+$ or free TMA can coordinate to the metallocene resulting in $[Cp_2ZrMe_2$-μ-$AlMe_2]^+$ species, which are also precursor to the uncoordinated cationic metallocene active site.[8–13] Finally, the MAO serves as well as a stabilizer for these active species, as shown by UV-Vis spectroscopy studies.[11,14] By carefully designing their ligands, monomer insertion can be controlled, making metallocenes a very versatile type of catalyst for the synthesis of polyolefins with defined microstructures.[1,15]

The metallocenes/MAO pair can be used for the polymerization of olefins in homogeneous systems. However, their immobilization on a support material is generally preferred for their use in existing industrial polymerization plants (which were designed for the previously discovered heterogeneous Ziegler-Natta and Phillips catalysts).[16,17] In fact, controlling the polymer morphology is generally a demanding task in polymerization processes – even more so in the absence of a solid support – and if not properly assessed, it can have disastrous consequences, the extreme case being complete reactor fouling.[17–19] An added advantage to fixing metallocenes on heterogeneous supports is that significantly less of the costly and pyrophoric MAO co-catalyst is needed to activate the metallocene, going from Al/Zr ratio of a few 1000 for homogeneous systems[20] to Al/Zr ratio of ~100 for supported ones.[14] The most common support employed to this scope is silica, as it is inexpensive, relatively chemically inert, and stable at high temperatures. Additionally, it can be synthesized in a variety of morphologies such as particle sizes, surface areas and pore sizes, making it a very versatile material that can be tuned according to the specific polymerization process requirements.[17,21–25]

Here, we investigate the modification of a commercial supported metallocene catalyst via titanation of its SiO_2 support (2-4 Ti wt.%), as described in the patent by Willocq *et al.*, which was reported to lead to an increase of olefins polymerization yields of up to 40% at industrially-relevant conditions, without affecting the polymer product properties.[26–28] However, the reasons behind the increased yields were not investigated in the reported literature. Hence, this study aims at elucidating the role played by such Ti modification of the SiO_2 support, which was obtained by surface modification of a commercial SiO_2 with titanium alkoxide, followed by heat treatment, resulting in a layer of TiO_x on the silica

[a] S. Zanoni, Prof. B. M. Weckhuysen
Inorganic Chemistry and Catalysis group
Institute for Sustainable and Circular Chemistry and Debye Institute for Nanomaterials Science, Utrecht University
Universiteitsweg 99
3584 CG Utrecht (The Netherlands)
E-mail: b.m.weckhuysen@uu.nl
[b] Dr. A. Welle, Dr. V. Cirriez
Catalysis and Products R&D
TotalEnergies Petrochemicals
Zone Industrielle C
7181 Feluy (Belgium)

Supporting information for this article is available on the WWW under https://doi.org/10.1002/cctc.202300221

surface and pore walls (further referred to as Ti/SiO_2). A similar titanation procedure has been used for decades with Cr-based Phillips catalyst systems.[29,30] This $Cr/Ti/SiO_2$, when activated by an aluminum-alkyl co-catalyst, can oligomerize ethylene into 1-alkenes which can then co-polymerize with ethylene, leading to a polymer product with a different chain structure having better processability properties than that obtained with the non-titanated Cr/SiO_2.[30] Ti modifications of the silica support are also used in newer generations of Ziegler-Natta catalyst materials, although in the co-presence of MgClx.[31] In this type of catalyst, the TiClx species are initially grafted on the silica and almost independent of the supported MgClx phase. However, the activation by alkyl-aluminum co-catalyst leads to radical reconstruction of the catalyst and most of the Ti sites become detached from the silica and highly dispersed in the MgClx phase, becoming essentially comparable to the classic Ziegler-Natta, i.e. not supported on silica.[32] In the case of metallocene-based olefin polymerization catalysts, the introduction of Ti in SiO_2 supports has also been reported in the literature. Jongsomjit *et al.* replaced a pure silica support with a SiO_2:TiO_2 (8:2) material, obtained by physical mixture of anatase with a commercial silica which led to a 60% increase in the copolymerization activity of ethylene with 1-hexene.[33,34] The improved activity was attributed to the decrease in steric hindrance due to TiO_2 playing the role of a spacer between the support and the catalyst as well as a site for anchoring MAO. However, the mechanical mixing of the two metal oxides is not expected to allow for a sufficiently strong anchoring of TiO_2 on the silica surface, while it is likely to lead to segregated TiO_2 particles. Furthermore, their conclusions did not take in consideration any potential other interaction between Ti sites and (co-) catalyst. More interestingly, Fisch *et al.* developed an immobilization method of Cp_2ZrCl_2 within a TiO_2–SiO_2 binary oxide via a non-hydrolytic sol-gel route to obtain a catalyst with 60% higher polymer yields.[35] The authors ascribed the higher polymerization activities to the interaction of Cp ligands with Ti–O–Ti structures, which would result in Zr centers with higher cationic character, favoring the monomer coordination step and found that activity increase was directly correlated to the concentration of 5-coordinated Ti^{4+} species, though no explanation was provided as to why.

In this study, a combination of spectroscopic techniques was used to understand the role of Ti in improving the polymerization catalytic activity of the modified Ti/SiO_2-supported zirconocene catalyst, investigating the commercial and modified $(Ti/)SiO_2$ supports, $Al/(Ti/)SiO_2$ precursors and $Zr/Al/(Ti/)SiO_2$ catalysts (Figure 1). Ethylene polymerization productivities were tested at high pressures in slurry-phase reactors and the thermal properties of the polymer obtained were measured by differential scanning calorimetry (DSC) and ^{13}C-NMR. To better assess differences in the kinetic behavior of

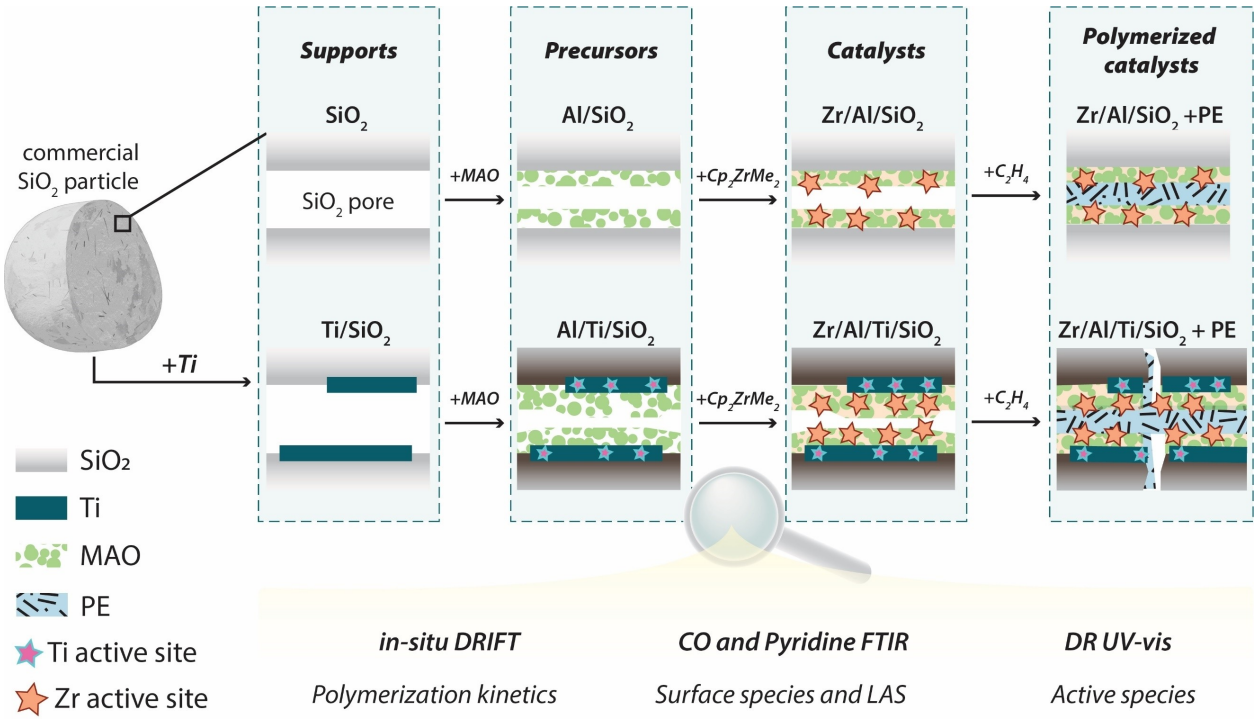

Figure 1. Schematic representation of the catalysts synthesis and characterization techniques employed to investigate the role of Ti species in the ethylene polymerization activity of Ti-modified metallocene-based olefin polymerization catalysts. The starting material was the same commercial silica for both SiO_2 and Ti/SiO_2-based catalyst materials under study. In the latter, Ti was deposited on the pore walls via impregnation of Ti alkoxide and subsequent heat treatment. Al/SiO_2 and $Al/Ti/SiO_2$ catalyst precursors were synthesized by impregnating methylaluminoxane (MAO) on the supports, followed by impregnation of Cp_2ZrMe_2, which led to the genesis of $Zr/Al/SiO_2$ and $Zr/Al/Ti/SiO_2$ catalysts. Polymerization kinetics of ethylene of the active catalyst materials were followed by *in-situ* Diffuse Reflectance Fourier Transform Infrared (DRIFT) spectroscopy. Fourier Transform Infrared (FT-IR) spectroscopy with CO and pyridine probe molecules was used to detect surface species and their Lewis acidity, a factor of major importance in the activation of metallocene centers. Finally, Diffuse Reflectance (DR) UV-Vis spectroscopy was used to assess the nature of Zr active centers and confirm the presence of reduced Ti^{3+} species.

the active catalysts, early-stage polymerization reactions were followed by *in-situ* Diffuse Reflectance Fourier Transform Infrared (DRIFT) spectroscopy. Fourier Transform Infrared (FT-IR) spectroscopy of the samples with pyridine as probe molecule was used to quantify the Lewis acidity of the surface species of supports, precursors and catalysts, a factor of major importance in the activation of metallocene centers, while CO as a probe molecule combined with FT-IR spectroscopy was used to better identify such surface species. Finally, Diffuse Reflectance (DR) UV-Vis spectroscopy helped with assessing the nature of Zr active centers and the oxidation state of Ti species, which could not be unambiguously determined by FT-IR spectroscopy.

The boosting role played by Ti in the olefin polymerization activity of the supported metallocene-based catalyst materials was proven to be complex. The improved catalytic performance of the modified catalyst was found to be related both to the presence of a Ti-based active site, second to the Zirconocene centers, as well as to a higher Lewis acidity in the titanated supported-MAO, which improved the activation of the Zr-based centers. The presence of a second active site was discovered when the modified Ti/SiO_2 support was found to be active in the polymerization of ethylene if in contact with an Al-based co-catalyst, such as MAO or TiBA, but in the absence of any metallocene sites. Such Ti active species were generated by reduction of the Ti/SiO_2 support with the methylaluminoxane (MAO) co-catalysts, which introduced oxygen vacancies (V_O) and Ti^{3+} species, as confirmed by probe molecule Fourier Transform Infrared (FT-IR) spectroscopy and UV-Vis Diffuse Reflectance Spectroscopy (DRS).

However, the measured productivity of the $Al/Ti/SiO_2$ support could only account for a portion of the overall productivity increase of the $Zr/Al/Ti/SiO_2$, when compared to the non-modified $Zr/Al/SiO_2$. Furthermore, early-stage kinetics of ethylene polymerization observed with *in-situ* DRIFT spectroscopy suggested that the Zr and Ti active sites present in the modified catalyst material did not act completely independent from each other. Pyridine and CO probe molecules FT-IR was then used to investigate this Ti–Zr synergy. It was found that the interaction of 5-coordinated Ti^{4+} sites with the MAO increased the Lewis acidity of the catalyst precursor $Al/Ti/SiO_2$, which is known to correlate to a better activation efficiency of the metallocene centers, that is, to a higher concentration of Zr active sites.[11,14]

Finally, the analysis of early-stage polymerization kinetics observed with *in-situ* DRIFT spectroscopy suggested that the presence of the Ti layer in the silica mesopores could improve the fragmentation efficiency of the support, leading to an easier access of ethylene monomer to the active sites. Because of the complexity of the phenomena at play, part 1 of this study, which is here reported, focuses on the characterization of the material active sites, while part 2 of this study will be dedicated to the differences in fragmentation between the two catalyst materials.[36]

Results and Discussion

Catalyst Materials Characterization

To verify potential changes introduced by the modification of the silica support with Ti, the morphology, structure, and composition of the supports, precursors, and catalysts were inspected via N_2-physisorption, Fourier Transform Infrared (FT-IR) spectroscopy and Inductively Coupled Plasma-Optical Emission Spectroscopy (ICP-OES) analysis. The Ti alkoxide added to the commercial silica was expected to anchor on the Si–OH on its external surface, as well as on its pore walls, forming a layer of TiO_2 after thermal treatment. As reported in Table 1, the elemental analysis by ICP-OES analysis revealed that the target content of 3.5 wt.% Ti was indeed reached in the samples under study. The N_2-physisorption data showed that such addition of Ti caused an increase in surface area from 231 to 241 m^2/g and a decrease of pore volume from 1.45 to 1.37 cm^3/g, with the average pore size going from 24 to 22 nm (as also shown in the pore size distribution reported in Figure 2a).

This indicates that the TiO_2 layer had an average thickness of 2 nm, while the slight increase in Brunauer-Emmett-Teller (BET) surface area suggests that such layer was not flat, but somewhat irregular. The FT-IR spectra of the unmodified SiO_2 support (Figure 2d) contained all the common vibrational bands of the silica support. Namely, the combination bands of the Si–O–Si network located in the region between 2080 and 1550 cm^{-1} and the Si–OH groups in the OH stretching region at 3800–3000 cm^{-1}. Here, the sharp peak at 3742 cm^{-1} is assigned to isolated Si–OH, while the broader bands centered at 3665 cm^{-1} and 3530 cm^{-1} are ascribed to intraglobular and

Table 1. Ti, Al and Zr content from Inductively Coupled Plasma-Optical Emission Spectroscopy (ICP-OES) analysis and Brunauer-Emmett-Teller (BET) surface areas, total pore volumes and average pore sizes from N_2-physisorption analysis.

Sample	Ti [wt.%][a]	Al [wt.%]	Zr [wt.%]	Al/Zr [Molar ratio]	BET surface area [m^2/g]	Tot. pore volume[b] [cm^3/g]	Pore size[c] [nm]
SiO_2	–	–	–	–	231	1.45	24
Ti/SiO_2	3.54	–	–	–	241	1.37	22
Al/SiO_2	–	12.83	–	–	291	0.70	17, 4, < 2
$Al/Ti/SiO_2$	2.21	14.38	-	-	300	0.57	14, 4, < 2
$Zr/Al/SiO_2$	–	12.13	0.43	95	260	0.67	17, < 2
$Zr/Al/Ti/SiO_2$	2.21	14.25	0.43	112	295	0.55	14, < 2

[a] Ti wt.% is lower in Al containing samples because of the 60% specific mass increase due to methylaluminoxane (MAO) addition. [b] Barret-Joyner-Halenda (BJH) desorption. [c] Pore size at Barret-Joyner-Halenda (BJH) curve maxima.

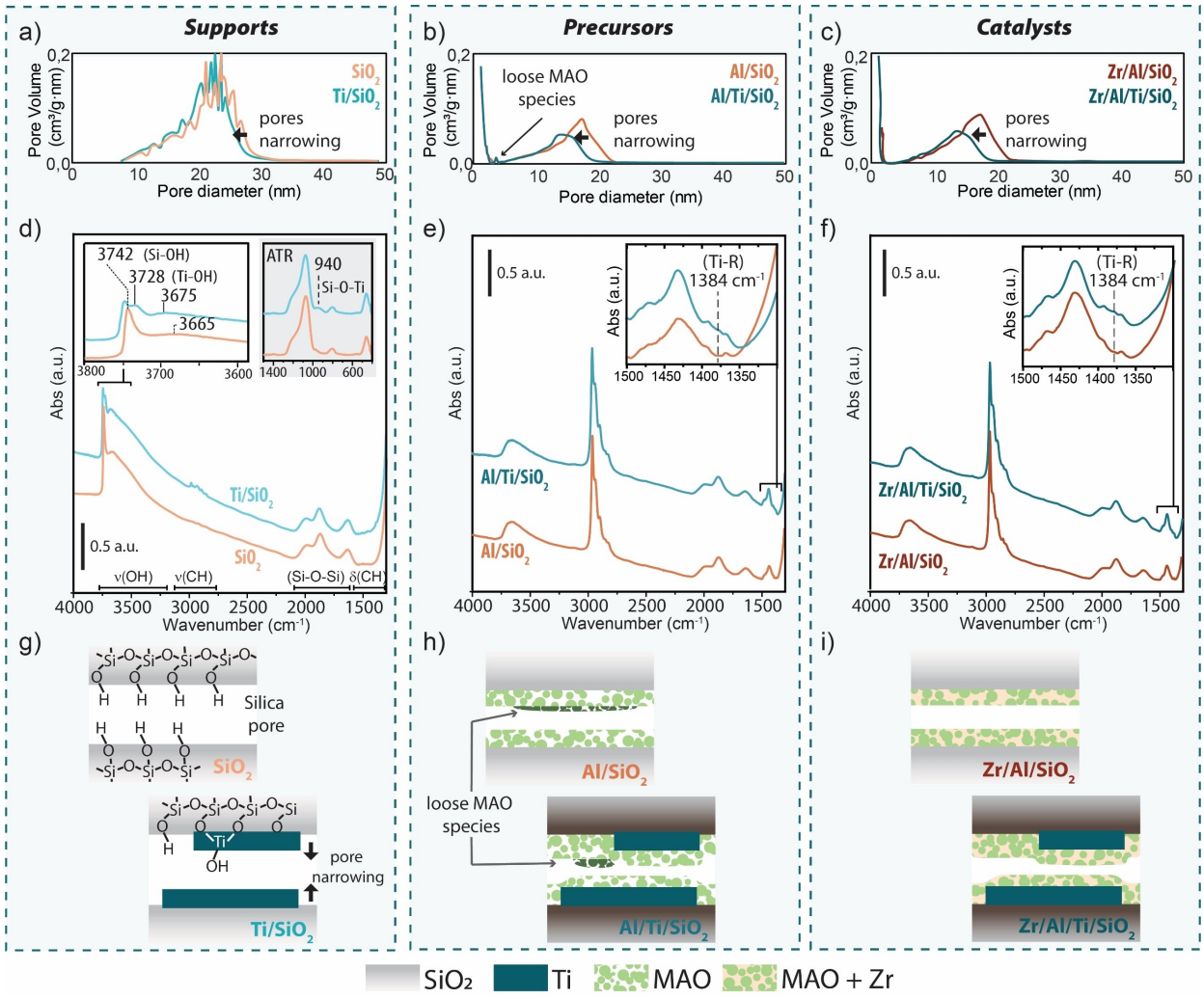

Figure 2. Barret-Joyner-Halenda (BJH) desorption curves derived from the N_2-physisorption measurements of a) SiO_2 and Ti/SiO_2 supports, b) Al/SiO_2 and $Al/Ti/SiO_2$ precursors, and c) $Zr/Al/SiO_2$ and $Zr/Al/Ti/SiO_2$ catalysts. d) FT-IR spectra of the two supports with zoom-in of the OH stretching region and of the ATR spectra at lower frequencies. e) FT-IR spectra of the two precursors and f) of the corresponding catalyst materials. All spectra were acquired at room temperature, under vacuum and plotted with an offset for clarity. g), h) and i) Corresponding schematic representation of the morphology changes within the pores of the SiO_2 and Ti/SiO_2-based supports, precursors, and catalyst materials.

vicinal OH groups, respectively.[37–39] Upon Ti modification of the SiO_2 support, the isolated Si–OH band decreased in intensity and blue-shifted to 3745 cm^{-1}, while a new peak at 3723 cm^{-1} appeared, which is ascribed to isolated Ti–OH, and a broad band centered at 3675 cm^{-1}, originating from vicinal Ti–OH groups.[39–41] This indicates that the Ti had indeed been grafted onto the SiO_2 support via condensation of its terminal Si–OH groups. Further confirmation of the Si–O–Ti bond formation was found at lower frequencies measured by Attenuated Total Reflectance (ATR) IR spectroscopy (inset Figure 2d), with the appearance of a broad band at 930–950 cm^{-1}.[40,42] The presence of these bonds, together with the appearance of the Ti–OH signal, indicate that the Ti alkoxide had, at least partially, hydrolyzed to TiO_2-like species. However, the presence of low intensity peaks in the CH stretching region, implies that traces of the alkoxide species of the Ti precursor were also still present. Moreover, since not all terminal Si–OH were consumed, we can deduce that the TiO_2 layer is not uniformly covering the entire surface of the silica support, but is rather present as discontinuous TiO_2 islands, as schematically depicted in Figure 2g, confirming the irregularity of the TiO_2 layer deduced by the analysis of the N_2-physisorption results.

The addition of MAO caused a decrease in average pore diameter of ~7 nm in both Al/SiO_2 and $Al/Ti/SiO_2$ samples (Table 1 and Figure 2b), indicating that the thickness of the MAO layer was rather similar in the two materials. On the other hand, as the pore volume of the support was already lower for the Ti/SiO_2 material, the addition of MAO led to a material with 20% smaller pore volume than the Al/SiO_2 support (i.e., 0.57 vs. 0.70 cm^3/g). The surface area increased for both samples, from 231 to 291 m^2/g for the SiO_2-supported MAO and from 241 to 300 m^2/g for the $Al/Ti\text{-}SiO_2$ precursor. This was due to MAO being present as a polymeric porous layer itself, which was also confirmed by the presence of microporosity and of an extra

peak centered at 4 nm, as evident in the Barrett–Joyner–Halenda (BJH) pore size distribution of the two precursors materials (Figure 2b).

The FT-IR spectroscopy analysis of the two catalyst precursor samples (Figure 2e) showed that the isolated Si–OH and Ti–OH species were consumed upon MAO impregnation, indicated by the disappearance of both 3742 and 3728 cm^{-1} bands. Furthermore, the overall signal in the OH stretching region decreased, implying that MAO consumed all isolated OH groups and some of the intraglobular and vicinal ones as well, presumably those more easily accessible.

The vibrational bands appearing in the υ(CH) and δ(CH) vibration regions in the range of 3000–2800 cm^{-1} and 1500–1300 cm^{-1}, respectively, are due to MAO derived alkyl groups. Panchenko *et al.* reported that the free $Al(CH_3)_3$ species (i.e., TMA) still present in MAO grafted on the silanols, to form $Si–O–AlMe_2$, while the MAO itself is only strongly adsorbed onto the silica surface.[43] In addition, such TMA can also interact with siloxane groups breaking the Si–O–Si bond in $Si–O–AlMe_2$ and $Si-CH_3$.[44,45] In the same way, the free TMA could also interact with the Ti–O–Ti moieties to form $Ti–O–AlMe_2$ and $Ti–CH_3$ species. As Si and Al have a very similar atomic mass, it would be virtually impossible to distinguish between $Si–CH_3$ and $Al–CH_3$ vibrations.[46]

As for $Ti–CH_3$, if present, the concentration is expected to be much lower than that of $Si–CH_3$ and $Al–CH_3$ species, therefore its signal could be overshadowed. Nonetheless, in the δ(CH) region an extra peak was found at 1384 cm^{-1} (inset in Figure 2e) for the catalyst precursor containing Ti ($Al/Ti/SiO_2$), which we therefore tentatively ascribe to the C–H bending vibration of Ti–R species. The elemental analysis revealed a loss in Ti loading in the precursor samples, from 3.5 to 2.2 in Ti wt.%, though only apparent. In fact, the specific mass of the samples increased considerably upon MAO impregnation (about 60%). Therefore, the Ti wt.% with respect to the SiO_2 mass is unvaried in the $Al/Ti/SiO_2$ sample, meaning that no Ti was lost, but rather that the Ti wt.% decrease is merely a reflection of the samples change in density. More interestingly, the Al content was 10% higher in the Ti-containing samples, which could imply that MAO is more prone to anchoring to the Ti–OH groups than to the Si–OH ones.

The BJH pore size distribution of the catalyst samples showed that the addition of zirconocene caused the 4 nm peaks to disappear for both catalyst materials (Figure 2c), suggesting that such porosity was linked to looser MAO species that were removed during the metallocene impregnation step. Since the total pore volume was unaffected, we can expect that the contribution of these lose species to the overall pore volume was minimal. However, the surface area decreased from 291 to 260 m^2/g and about 6% of the Al content was lost (from 12.83 to 12.13 wt.%) in the SiO_2-based catalyst after zirconocene impregnation (i.e., the $Zr/Al/SiO_2$ system), indicating a partial removal of MAO during the rinsing step. On the other hand, in the Ti-modified catalyst (i.e., the $Zr/Al/Ti/SiO_2$ system), the Al loss was below 1%, once again indicating a stronger interaction of MAO with the TiO_2 layer of the support. The Zr loading was found to be equal between the two samples, namely 0.43 wt.%, but the higher loading of MAO in the $Zr/Al/Ti/SiO_2$ catalyst material resulted in a higher Al/Zr ratio, which is expected to be beneficial to the zirconocene activation. The FT-IR spectra of the catalysts (Figure 2f) do not show any visible differences from the corresponding spectra of the two precursors (Figure 2e) as the concentration of the metallocene are low and the CH vibration of its ligands overlap with more intense MAO derived CH_3 groups.

In summary, as schematically illustrated in Figure 2g–i, the Ti modification of the SiO_2 support resulted in the formation of a discontinuous TiO_2 layer grafted on the terminal Si–OH groups of the commercial support, which narrowed the average pore size of the titanated samples and with a more strongly bound MAO, ultimately leading to a Ti-containing catalyst material with narrower pores and higher Al/Zr ratio. Such morphological and composition differences already hint at two potential benefits resulting from the Ti modification of the support, namely a possible earlier fragmentation of the catalyst, as smaller pores would fill sooner, together with the presence of a higher concentration of Zr active sites, which could accelerate the olefin polymerization reaction. The differences in fragmentation between the two catalyst materials are investigated in more detail in part 2 of this manuscript,[36] while in the following section we focus on the difference in the nature and concentration of the active sites.

Catalyst Materials Testing

The activities of supports, precursors, and catalysts were tested for the polymerization of ethylene in the slurry-phase and the results are summarized in Table 2. The results obtained with the supported zirconocenes showed that the presence of Ti in the support caused a ~35% increase in polyethylene (PE) yields, compared the non-modified $Zr/Al/SiO_2$ catalyst. Ethylene polymerization measurements of the support and precursors were performed as a blank experiment, but led to the discovery that

Table 2. Yield of Polyethylene (PE) per gram of catalyst material obtained in heptane slurry-phase reaction at 9 bar of ethylene pressure, 55 °C in 1 h, with tri-isobutylaluminum (TiBA) as moisture impurities scavenger, calculated as average of three measurements.

Sample	Productivity [gPE/gCat]	Relative Productivity[a]
$Zr/Al/SiO_2$	94.7 ± 0.1	1
$Zr/Al/Ti/SiO_2$	128.6 ± 0.2	1.36
Al/SiO_2	–	–
$Al_{TiBA} + SiO_2$[b]	–	–
$Al/Ti/SiO_2$	23.7 ± 0.2	0.25
$Al_{TiBA} + Ti/SiO_2$[b]	25.8 ± 0.2	0.27
SiO_2[c]	–	–
Ti/SiO_2[c]	–	–

[a] Relative productivity to that of the $Zr/Al_{MAO}/SiO_2$ catalyst material. [b] Though TiBA was used as scavenger in the other reactions, the label Al_{TiBA} is here used to indicate that TiBA was acting as Al-based co-catalyst, while no methylaluminoxane (MAO) was present. [c] No TiBA was added to these reaction mixtures to confirm that the Ti/SiO_2 support is inactive by itself, when either Al-based co-catalysts (i.e., MAO or TiBA) are present.

the modified precursor Al/Ti/SiO_2 support was also active for ethylene polymerization, even in the absence of the main Zr active center. Ethylene polymerization measurements were performed with tri-isobutylaluminum (TiBA) in the reaction mixture as moisture scavenger, a common practice in olefin polymerization processes where the smallest traces of water or air could poison the catalyst material. Under these experimental conditions, also the Ti/SiO_2 support was found to be active. However, if no TiBA was added to the reactor, no activity was detected for the modified support.

The polyethylene produced were analyzed by DSC and ^{13}C-NMR, to exclude the possibility that the Ti active site could synthesize a second α-olefin to be inserted in the PE chain and introduce branching. In fact, this was the case for the Cr/Ti/SiO_2 Phillips-type ethylene polymerization catalyst reported by Cicmil *et al.*, in which the Ti/SiO_2 support was obtained by a similar synthesis procedure as the one used in this work.[30] As more extensively reported in the SI, these analyses showed that the PE produced by the commercial and modified catalyst, as well ad that produced by the active Al/Ti/SiO_2 support, were all linear, non-branched HDPE.

Thus, the modified Ti/SiO_2 support possess Ti species that can be activated toward the polymerization of ethylene by reducing and alkylating co-catalysts, such as methyl-aluminoxane (MAO) or tri-isobutylaluminum (TiBA), and that such species produce a polymer that is not distinguishable from that produced by the Zr active sites. It must be also noted that the Ti/SiO_2 support with added TiBA (Al_{TiBA} + Ti/SiO_2) showed ~9% higher activity than the Al/Ti/SiO_2 support. We expect that the formation of active Ti sites is linked to the interaction with the free trimethyl-aluminum (TMA) present in MAO, based on the easier accessibility of such species to the surface sites of Ti/SiO_2. This would explain the higher activity of Al_{TiBA} + Ti/SiO_2, since TMA accounts for only a small fraction of the total Al in MAO, while all of the TiBA molecules can potentially interact with Ti to activate it. Although one could argue that TiBA is also present (as a scavenger) in the ethylene polymerization experiment with Al/Ti/SiO_2, the presence of bulky MAO hinders the access of TiBA to the Ti sites, again explaining the better performance of the Al_{TiBA} + Ti/SiO_2 material.

With Ti centers acting as a second family of active sites next to the Zr centers in the Zr/Al/Ti/SiO_2 material, it is evident that the improved catalytic performance is mainly due to the higher concentration of active sites (i.e., both the Ti and Zr centers) when compared to the Zr/Al/SiO_2 material, which activity only relies on the presence of Zr sites. However, the PE yield obtained by the Zr/Al/Ti/SiO_2 material was higher than the sum of that obtained with the Al/Ti/SiO_2 support (where only Ti centers exist) and that of Zr/Al/SiO_2 (where only Zr centers are present). Specifically, a third of the ~35% boost in activity is not accounted for if we only consider the contribution of the additional Ti active sites. This suggests that the co-existence of Ti and Zr has a secondary boosting effect on the catalytic performance of the Zr/Al/Ti/SiO_2 material which is further investigated later in this study.

Early-Stage Kinetics of Ethylene Polymerization as Assessed by Infrared Spectroscopy

The PE yields of the different catalyst materials at specific reaction conditions, which have been discussed in the previous section of this study gave a good indication of the relative average ethylene polymerization activity of the different catalysts. However, reaction rates are not constant over time, due to chemical phenomena (e.g., monomer insertion, chain propagation and chain termination) as well as physical phenomena (e.g., diffusion of monomer towards the active sites and fragmentation of the catalyst materials). *In-situ* spectroscopic studies are a valuable tool to explore these events and to better assess potential differences in the catalyst materials under study. More specifically, *in-situ* Diffuse Reflectance Infrared Fourier Transform (DRIFT) spectroscopy was used to measure the rate of polymer growth on the catalyst particles, while flowing ethylene through the catalyst bed. A more detailed description of the experimental procedure and data analysis for this technique can be found in the SI.

The early-stage ethylene polymerization rates of the two catalyst materials Zr/Al/SiO_2 and Zr/Al/Ti/SiO_2 as well as that of the Al/Ti/SiO_2 active precursor material were compared. as reported in Figure 3. The kinetic curves of the two catalyst materials containing zirconocene (i.e., the Zr/Al/SiO_2 and Zr/Al/Ti/SiO_2 systems) followed a similar trend (Figure 3a,b). The initial ethylene polymerization rates were faster and reached a maximum at 2 min, peaking at 313 min^{-1} and 217 min^{-1} for Zr/Al/Ti/SiO_2 and Zr/Al/SiO_2, respectively, making the initial ethylene polymerization rate ~45% higher when in the presence of Ti. On the other hand, the curve of the Al/Ti/SiO_2 sample had a lower initial ethylene polymerization rate, reaching a maximum of only 130 min^{-1} and at a later time (i.e., 5 min).

For the Zr-containing samples, ethylene polymerization slowed down for a few minutes, but underwent a second sudden acceleration. The cause for such rate deceleration is attributed to ethylene diffusion limitations to the active sites induced by the formation of PE,[47] while the following acceleration is induced by fragmentation of the catalyst particles, which expose their active sites that had yet to participate in the ethylene polymerization, explaining the rate exponential increase. It is evident from Figure 3b that this rate acceleration occurred earlier for the Zr/Al/Ti/SiO_2 catalyst (9 min compared to the 12 min for the SiO_2/MAO/Zr catalyst) and that the rate acceleration itself was higher, as evidenced by the steeper slope of the Zr/Al/Ti/SiO_2 curve at this stage (49.7 min^{-2} vs. 13.4 min^{-2}). Eventually, this was accompanied by an expansion of the catalyst bed and saturation of the FT-IR signal, at which point analysis of the DRIFT spectra was no longer valid to obtain relevant kinetic curves. Hence, those points were excluded from the calculation of the rates. Nevertheless, we must note that both signal saturation and catalyst bed expansion occurred earlier in the Zr/Al/Ti/SiO_2 sample. The kinetic curve of the Al/Ti/SiO_2 sample did not experience such rate acceleration, but instead decreased for several minutes until it reached a steady-state rate of 30 min^{-1}. Despite this, ethylene polymerization never came to a halt, which indicates

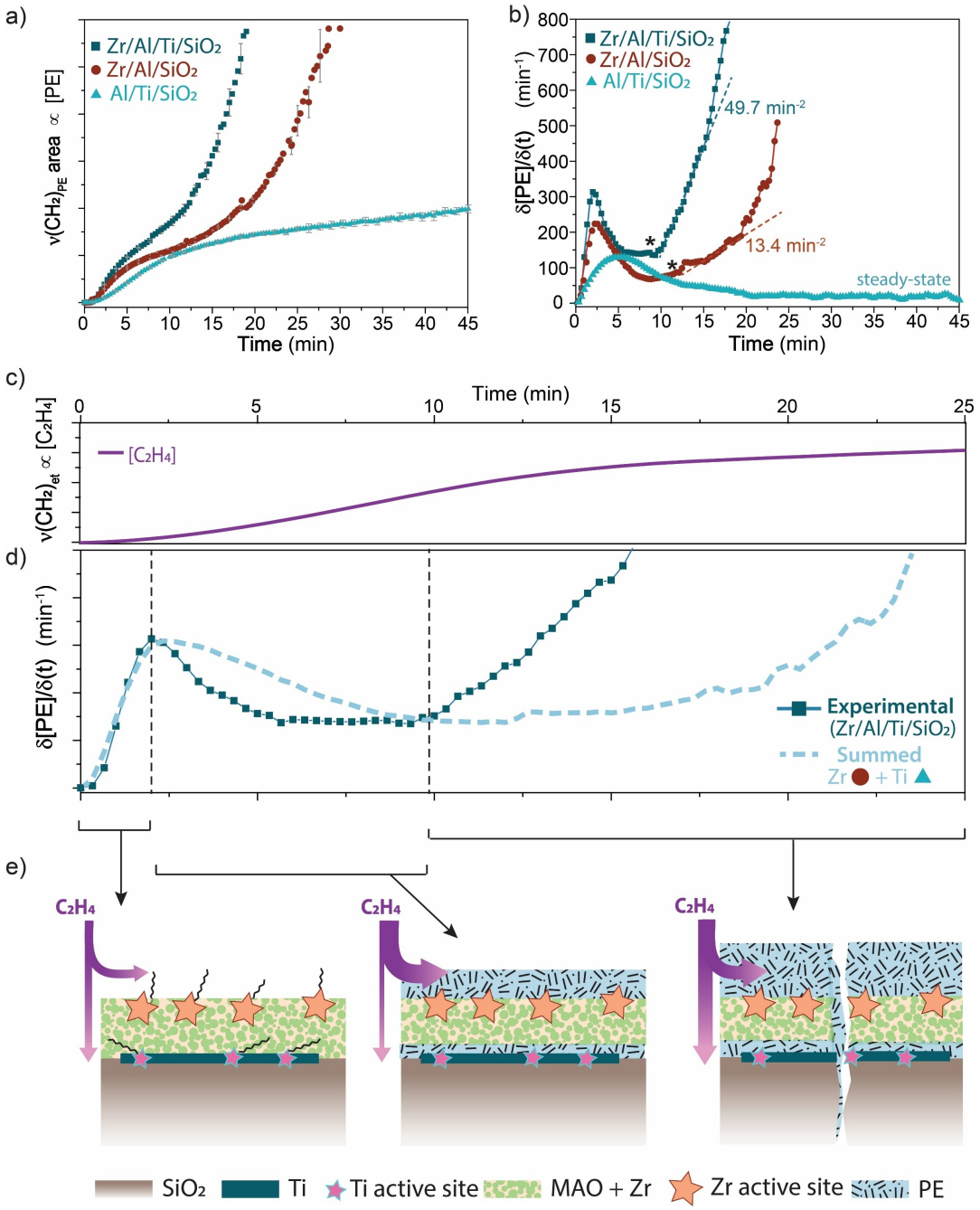

Figure 3. Ethylene polymerization reaction kinetics probed with *in-situ* Diffuse Reflectance Infrared Fourier Transform (DRIFT) spectroscopy. a) Area of the $\upsilon(CH_2)$ FT-IR stretching vibration of the growing polyethylene (PE) chains, proportional to [PE] accumulating over time. The grey vertical bars represent the standard deviation from the average curve obtained from multiple experiments with the same catalyst sample. b) First derivative of the curves in (a), which corresponds to the evolution of the ethylene polymerization rate over time. Fragmentation of the catalyst starts at *. c) Ethylene concentration over time, measured as the sum of the $\upsilon(CH_2)$ FT-IR stretching vibration peaks area of ethylene. d) Polymerization rate of the $Zr/Al/Ti/SiO_2$ catalyst material compared to the sum of the polymerization rates for the $Zr/Al/SiO_2$ and $Al/Ti/SiO_2$ materials (dashed line). The kinetic profiles are divided into three stages, which are schematically depicted in e).

that ethylene insertion to the Ti active site was steadily occurring for the reaction time observed.

Figure 3d compares the experimental rate curve of the $Zr/Al/Ti/SiO_2$ catalyst (continuous line) to the mathematical sum of the curves for the $Al/Ti/SiO_2$ support and the $Zr/Al/SiO_2$ catalyst (dashed line). The summed curve represents what could be expected for the $Zr/Al/Ti/SiO_2$ sample if the Ti and Zr active sites acted entirely independent from each other and was therefore compared to the experimental rate curve of such sample. As evident from the differences between the summed and the experimental curve, there should be a synergetic effect between the two sites at play. To better understand such differences, the

rate curves in Figure 3d were divided into three stages. In the first stage at the beginning of the ethylene polymerization reaction, the summed curve matched the experimental one of $Zr/Al/Ti/SiO_2$, reaching the same maximum rate value at the same time. At this point, ethylene was present at relatively low concentrations, as it just started flowing through the catalyst bed, making it the rate-limiting factor. At this regime, we cannot observe possible synergetic effects; hence, the summed curve matched the experimental one of the $Zr/Al/Ti/SiO_2$ catalyst material. In the second stage, where polymer accumulation caused diffusion phenomena, the experimental rate curve was lower than the summed one. As the intrinsic activity of Zr centers is higher than that of Ti site, the formers were depleting ethylene and contributing further to its slow diffusion towards the Ti sites, which are buried deeper into the catalyst material, under the MAO layer. Therefore, the Ti active centers will have an apparent lower ethylene polymerization rate due to lower ethylene concentration in their surroundings, thereby contributing to the lowering of the experimental rate curve.

This was not the case in the summed curve, where the two active sites are independent, each having comparable access to ethylene. In the third stage, the situation reversed, with the experimental rate becoming increasingly higher than that of the theoretical sum. Here, ethylene has reached a steady flow, and the $Zr/Al/Ti/SiO_2$ catalyst material started to fracture. Hence, both ethylene concentration and slow diffusion were no longer rate-limiting factors, or at least to a considerably lower extent than in the previous stages of the ethylene polymerization process. As the experimental curve was exponentially faster than the sum, we can infer that there must be a synergetic effect between Zr and Ti active sites. As fragmentation occurred earlier for the $Zr/Al/Ti/SiO_2$ catalyst than for the $Zr/Al/SiO_2$ catalyst (Figure 3b), an earlier or more efficient catalyst particle fragmentation is also contributing to the overall activity improvement induced by the presence of Ti in the support material However, the rate curve slope for the $Zr/Al/Ti/SiO_2$ catalyst was much steeper than the sum curve, suggesting that the co-presence of Ti and Zr also lead to the creation of active sites with intrinsically higher activity, or to a higher concentration of Zr active sites. To explore this aspect, the surface site species were investigated with probe molecule FT-IR spectroscopy, as reported in the next section.

Acidity and Surface Species Measurements with Probe Molecule Infrared Spectroscopy

Pyridine Fourier Transform-Infrared Spectroscopy

The FT-IR spectra of the different materials under study, after the adsorption of pyridine and the subsequent evacuation at 150 °C, are reported in Figure 4, together with the frequency ranges of the vibration modes for pyridine interacting with either Brønsted or Lewis acid sites (further labeled as Py-BAS and Py-LAS). The quantification of LAS is reported in Table 3, calculated from the integral of the band assigned to the 19b

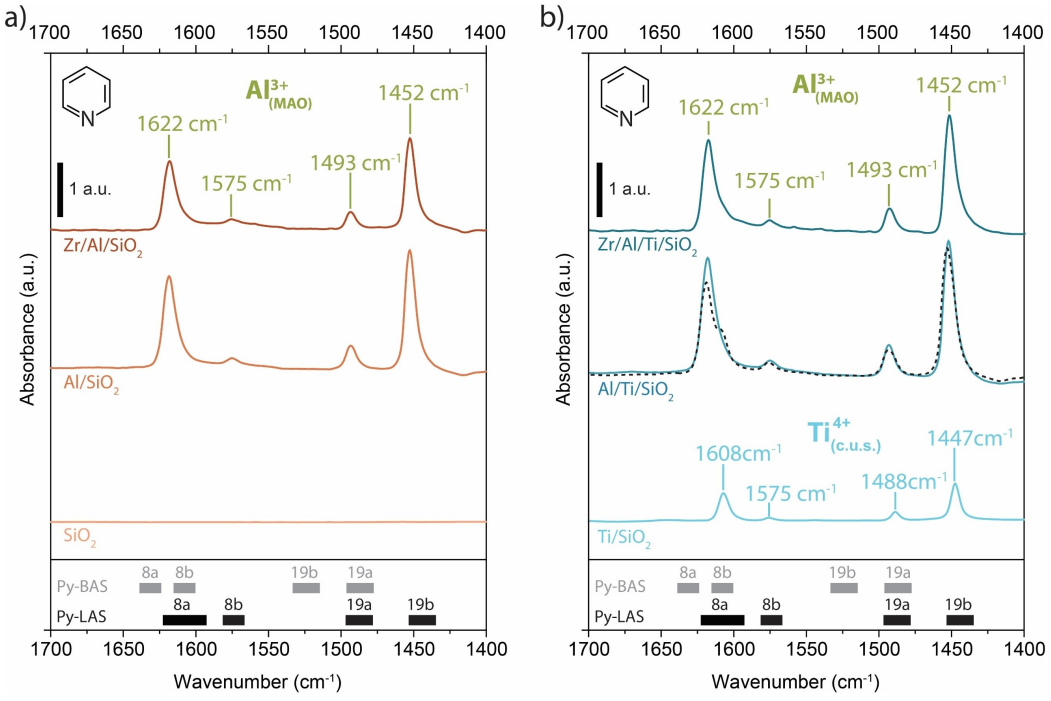

Figure 4. Fourier Transform-Infrared (FT-IR) spectra upon pyridine adsorption and subsequent desorption treatment at 150 °C for 30 min, while evacuating of a) SiO_2-based and b) Ti/SiO_2-based supports, precursors, and catalyst materials. The dashed-line spectrum in figure (b) is the sum of the Al/SiO_2 and Ti/SiO_2 spectra, overlapped to the $Al/Ti/SiO_2$ spectrum to aid comparison. The spectrum prior pyridine adsorption was first subtracted from each pyridine FT-IR spectrum, and the results are plotted with an offset for clarity. The ranges of the pyridine ring vibration when interacting with Brønsted and Lewis acid sites are also indicated for reference at the bottom of both graphs.

Table 3. Quantification of the total Lewis Acid Sites (LAS) concentration, calculated from the area of the 19b ring vibration of Py-LAS of each sample and the density of the sample wafer (mg/cm^2).

Sample	LAS [mmol/g]	Sample	LAS [mmol/g]
SiO_2	0.00	Ti/SiO_2	0.07
Al/SiO_2	0.34	$Al/Ti/SiO_2$	0.42
$Zr/Al/SiO_2$	0.26	$Zr/Al/Ti/SiO_2$	0.36

vibrational mode of pyridine interacting with LAS, as proposed in the literature.[14,43]

As evidenced by the FT-IR spectrum of the SiO_2 support in Figure 4a, pyridine was completely desorbed from the commercial support, already after the initial evacuation of the cell and even before the temperature was raised to 150 °C, confirming that its surface sites, including Si–OH species, were non-acidic. On the other hand, the spectra of the Ti/SiO_2 support, as shown in Figure 4b, reveal four bands at 1608, 1575, 1488 and 1447 cm^{-1}, which are related to ring vibrations of pyridine interacting with Ti^{4+} coordinatively unsaturated sites ($Ti_{c.u.s.}$), having Lewis acid character and at a concentration of 0.07 mmol/g (Table 3).[41,48–50] Ti atoms in the bulk of stoichiometric TiO_2 are coordinated to 6 oxygens ($Ti_{6\text{-}c}$), while surface and edges Ti sites will have a lower coordination (i.e., coordinatively unsaturated sites – c.u.s.), namely 5-fold Ti and 4-fold Ti, which gives them Lewis acidic character. Since only one narrow 8a peak was present in the FT-IR spectrum of the Ti/SiO_2 material, it is plausible that pyridine could not distinguish between the two c.u.s or that one was more abundant or more accessible than the other by the bulky pyridine molecule.

As for Brønsted acidity, which could be generated from the OH groups shared between Si and Ti atoms, the lack of bands at 1640 and 1540 cm^{-1} indicates the absence of such Brønsted sites in the support oxide under study. This finding corresponds to what was found in the literature, where TiO_2/SiO_2 oxides obtained via similar impregnation routes, were shown to possess Brønsted acid sites only after the oxide was contacted with water vapor[48] or if higher loadings of Ti were grafted on the SiO_2.[41]

The impregnation of the MAO co-catalyst introduced Lewis acidity in both support materials, as evidenced by the presence of the bands located at 1622, 1575, 1493 and 1452 cm^{-1} in the FT-IR spectra of the Al/SiO_2 and $Al/Ti/SiO_2$ support materials (Figure 4), ascribed to pyridine coordinated to tetrahedral Al^{3+} LAS from the MAO.[14] The red-shifted (15 cm^{-1}) position of these 8a bands when compared to those found for pyridine coordinated to the bare titanated support, indicates that the Al^{3+} sites have a stronger Lewis acid character than the $Ti_{c.u.s.}$. Interestingly, the bands assigned to pyridine interacting with $Ti_{c.u.s.}$ are no longer visible in the spectrum of the $Al/Ti/SiO_2$ material. As the py-Al^{3+} bands are very close in frequency and much more intense, it is possible that such peaks would be eclipsed. However, when we summed the spectra of Al/SiO_2 with that of Ti/SiO_2, we obtained a spectrum with an 8a band at 1622 cm^{-1} having a visible shoulder at 1608 cm^{-1} (this can be seen in the dashed-line spectrum in Figure 4b), which was not present in the measured spectrum of the $Al/Ti/SiO_2$ sample. This indicates that the $Ti_{c.u.s.}$ species of the support were, at least partially, consumed by the MAO. Furthermore, the total concentration of LAS in the $Al/Ti/SiO_2$ sample (i.e.,0.42 mmol/g) was greater than the sum of Ti/SiO_2 (i.e., 0.07 mmol/g) and Al/SiO_2 (i.e., 0.34 mmol/g). This suggests that the $Ti_{c.u.s}$ species were not just consumed by the MAO, but that their interaction led to a supported co-catalyst with a total higher concentration of Lewis acid sites than in the non-modified SiO_2 supported precursors. Since activation of metallocene centers is linked to the Lewis acidity of its co-catalyst, a higher concentration of LAS is expected to lead to a more efficient activation of metallocenes, i.e., a higher concentration of active Zr centers. In fact, Velthoen *et al.* showed that the Lewis acidity of the supported MAO precursors measured by pyridine FT-IR spectroscopy directly correlated to the activity of the catalysts, hence to the concentration of the active metallocene centers.[14]

The nature of the acid sites was not altered by the addition of the zirconocene, as seen in the top FT-IR spectra of Figure 4. However, the intensity of the bands and therefore the concentration of LAS, decreased both for the Ti/SiO_2 and SiO_2-based catalyst materials. This behavior has been observed before and was ascribed to the MAO LAS being partially consumed by the zirconocene, while the Zr LAS themselves being too low in concentration to be detected.[14] For that reason, the concentration of LAS in the precursor systems is a better indication of catalyst activation efficiency than that of the catalyst samples themselves. However, one observation is worth noting. That is, the loss in LAS concentration in the $Zr/Al/SiO_2$ material is more pronounced than in the $Zr/Al/Ti/SiO_2$ material (from 0.34 to 0.26 mmol/g and from 0.42 to 0.36 mmol/g, respectively), matching the observation by ICP-OES where the $Zr/Al/SiO_2$ catalyst had suffered a greater drop in Al wt.% from its Al/SiO_2 precursors (Table 1), giving another confirmation of the stronger interaction of MAO to the support thanks to the Ti-modification.

Summarizing, FT-IR spectroscopy on the samples after pyridine adsorption showed that the titanation of the commercial SiO_2 support introduced $Ti_{c.u.s.}$ species with LAS character, which upon MAO impregnation were partially consumed by the co-catalyst. The interaction between these Ti species with the MAO co-catalyst led to a more strongly bound MAO and an $Al/Ti/SiO_2$ catalyst precursor material with a higher concentration of LAS that in the non-modified Al/SiO_2 sample. We are of the opinion that these LAS contribute to the higher activity of the Ti-modified catalyst samples, as a higher LAS concentration of the catalyst precursors is linked to a better activation of the metallocene, i.e., a higher concentration of active Zr sites.

CO Fourier Transform-Infrared Spectroscopy

While pyridine FT-IR was used to quantify the Lewis acidity of the catalyst materials, CO FT-IR was employed to better assess their surface species, in particular to identify the nature of the Ti-based active site. Figure 5 reports the FT-IR spectra of the SiO_2 and Ti/SiO_2-based supports, precursors, and catalyst samples after adsorption of CO as probe molecule. More

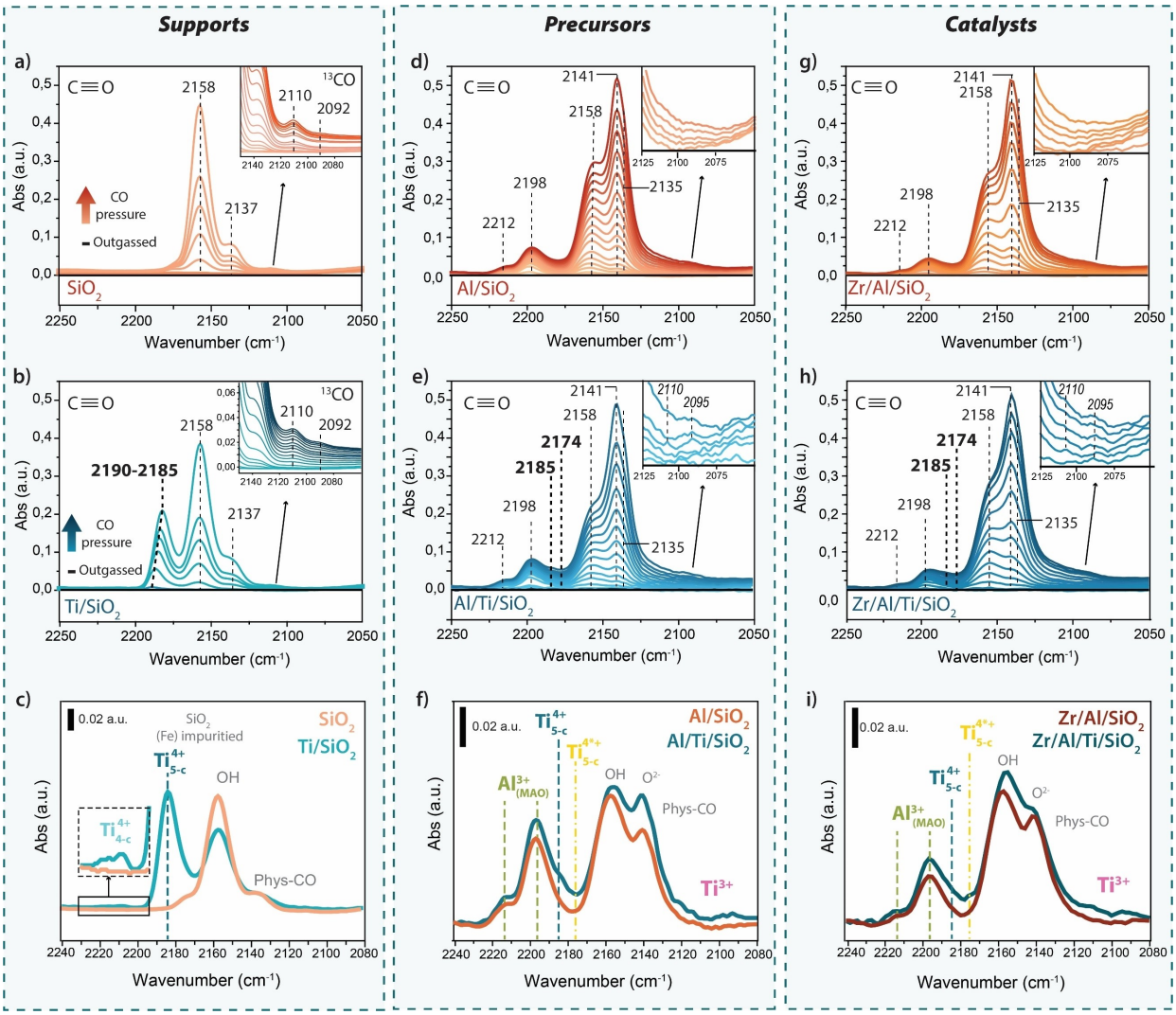

Figure 5. Fourier Transform-Infrared (FT-IR) spectra upon CO adsorption at 85 K. a) SiO_2 and b) Ti/SiO_2 with increasing pressure of CO and in c) the overlap of two spectra of SiO_2 and Ti/SiO_2 at equal CO pressure; d) SiO_2/MAO and e) Ti/SiO_2/MAO with increasing pressure of CO and overlap of two spectra at equal CO pressure for comparison in (f); g) SiO_2/MAO/Zr and h) Ti/SiO_2/MAO/Zr with increasing pressure of CO and overlap of two spectra at equal CO pressure for comparison in (i).

specifically, the FT-IR spectra are reported with increasing CO pressure for all samples under study. In addition, to aid the comparison between the modified and commercial samples, two CO FT-IR spectra of each support, precursor and catalyst at equal CO pressure are overlapped in the third figure of each series to facilitate comparison and hence their interpretation.

The adsorption of CO on SiO_2 (Figure 5a) resulted in two main bands, located at 2137 cm^{-1} and 2158 cm^{-1} and which correspond to physisorbed CO and CO interacting with OH, respectively.[39,40] A small peak was also present at 2170 cm^{-1} likely due to the presence of Fe impurities in the commercial silica employed.[51] The Ti/SiO_2 sample (Figure 5b) showed the same two absorption bands of physisorbed CO (2137 cm^{-1}) and H-bonding of CO with surface OH groups (2158 cm^{-1}) as those found in the spectrum of the non-modified SiO_2 support. Though literature studies of CO adsorption of pure TiO_2 anatase nanocrystal have reported lower frequency values of CO on Ti–OH, namely 2154–2157 cm^{-1},[52,53] it was concluded that CO cannot distinguish between non-acidic Si–OH and Ti–OH groups in mixed TiO_2/SiO_2 materials,[54] as it is found to be the case in the support material studied here.

Furthermore, an additional absorption band arose, which frequency shifted from 2190 cm^{-1} to 2185 cm^{-1} with increasing CO pressure, assigned to 5-coordinated Ti^{4+} as found both in the (101) faces of TiO_2 anatase,[52,53] and in the (110) faces of rutile.[55–57] The shift to lower frequencies with increasing CO coverages indicates dipole coupling of neighboring adsorbed CO. This implies that multiple (5-c)Ti^{4+} are located in close proximity, confirming that titania is present as a layer, rather than isolated Ti moieties. These surface sites have a Lewis acid character and are responsible for the absorption band at 1608 cm^{-1} present in the pyridine FT-IR spectrum in the previous section. A very small and broad signal at higher frequencies (~2210 cm^{-1}), characteristic of surface sites with

larger polarizing power, is assigned to lower coordination species, i.e., 4-coordinated Ti^{4+} centers, located on defects or edges (zoom-in Figure 5c).[53] The intensity of this band was very low, in agreement with the expected low concentration of such surface sites. At higher CO coverages, two additional peaks appeared at 2110 cm^{-1} and 2092 cm^{-1} for both SiO_2 and Ti/SiO_2 supports (Figure 5a–b inset), which intensity was directly proportional to that of 2158 cm^{-1} and 2137 cm^{-1} peaks, and are ascribed to the naturally occurring ^{13}CO interacting with OH and physisorbed ^{13}CO, respectively.[53,58]

The FT-IR spectra of the Al/SiO_2 sample after CO adsorption (Figure 5d) confirmed the presence of Lewis acid sites, with the appearance of new peaks at 2212 cm^{-1} and 2198 cm^{-1}, deriving from the Al centers of the MAO co-catalyst. Although pyridine-FT-IR spectroscopy did not allow for such distinction, the presence of these two peaks in the CO FT-IR spectra suggested that Al species in MAO possess two types of LAS with different strengths, corresponding to previous findings reported in the literature.[13,14,43] The 2198 cm^{-1} absorption band is ascribed to the presence of weakly Lewis acidic Al^{3+} of $OAlMe_2$ moieties, while the less intense absorption band at 2212 cm^{-1} is attributed to moderate Al^{3+} Lewis acid sites, of mono-methylated O_2AlMe as the electron-withdrawing inductive effect of the two oxygen atoms makes this aluminum species a stronger Lewis acid site.[13,14,43] Notably, the absorption band of physisorbed CO was shifted to lower frequencies, 2135 cm^{-1} ($\Delta\upsilon = -2$ cm^{-1}), and a new absorption band at 2141 cm^{-1} appeared, which was not present in the bare support samples. Such changes are due to the presence of MAO, which introduced microporosity in the sample. This caused the physisorbed probe molecules to condense in the pores as liquid-like CO, decreasing its vibration frequency. On the other hand, O^{2-} species of the MAO with Lewis base character can interact with CO, resulting in the band at 2141 cm^{-1}.[59]

Figure 5e shows the FT-IR spectra of CO interacting with the $Al/Ti/SiO_2$ material at increasing CO coverage, though differences caused by the presence of Ti are more evident in Figure 5f, where a spectrum of the Al/SiO_2 material and one of $Al/Ti/SiO_2$ material at the same CO pressure were overlapped for ease of comparison. The intensity of the bands at 2198 and at 2212 cm^{-1} of moderate and weak Al^{3+} LAS were higher for the $Al/Ti/SiO_2$ sample. This confirmed the observation of the pyridine FT-IR analysis as well as the ICP-OES measurements, which is that the presence of Ti surface species in the modified metal oxide led to higher concentration of Al-based Lewis acid sites. Furthermore, the weak LAS band in the spectrum of the $Al/Ti/SiO_2$ sample possessed a shoulder with a local maximum at 2185 cm^{-1}. This band position corresponded to that of CO adsorbed on the (5-c)Ti^{4+} present in the Ti/SiO_2 support, indicating that some of these species were still available for CO adsorption after MAO impregnation.

The reducing properties of MAO can be expected to reduce some of the Ti^{4+} to Ti^{3+} species. The change in color of the Ti/SiO_2 support from white to dark yellow-grey after its impregnation with MAO, indicates that reduction of Ti has indeed taken place. In fact, unlike stoichiometric TiO_2, which absorbs in the UV region and is therefore white, reduced TiO_2 containing oxygen vacancies and Ti^{3+} (d^1) species absorbs visible light at lower energies, with a resulting color that depends on the amount of oxygen vacancies in the sample.[60,61] This was also confirmed by UV-Vis-DRS spectroscopy, as more extensively reported in the SI. In fact, the $Al/Ti/SiO_2$ sample presented a strong absorption signal of visible light in the *d-d* charge transfer region, which was not present in the bare Ti/SiO_2 support. This confirms the occurrence of reduced Ti^{3+} (d^1) species, as a consequence of the interaction of either MAO or TiBA Al-based co-catalyst with the modified Ti/SiO_2 support. On the other hand, probing such reduce species with CO-IR is less trivial. In the literature, reduced CO was shown to adsorb on reduced TiO_2 at surface Ti sites in the vicinity of the oxygen vacancy (V_O), though not on the vacancy itself, resulting in an absorption band at 2178 cm^{-1} in reduced single crystals of rutile TiO_2 and at 2174 cm^{-1} in bulk rutile TiO_2 powders.[55,56,62] In the comparison of Figure 5f between Al/SiO_2 of $Al/Ti/SiO_2$, the titanated precursor spectrum showed higher light absorption at ~2174 cm^{-1}, though no clear peak could be identified. Nonetheless, this absorption band is assigned to (5-c)Ti^{4*+}, where the * symbol indicates the vicinity to the electron density of an oxygen vacancy, though its exact nature and presence will be discussed later.

If CO were to adsorb directly at the O vacancy, i.e., on the Ti^{3+} surface species, the π-back-donation to CO of the *d* orbital unpaired electron in the Ti coordination sphere would cause a red-shift in the vibrational frequency of CO. In the literature, Ti^{3+} has been reported to provide an absorption band located at 2115 cm^{-1} in reduced TiO_2[40] and located at 2091–2076 cm^{-1} in Ziegler-Natta TEA/TiClx/$MgCl_2$ catalyst systems,[63,64] while DFT calculations estimated frequencies lower than 2000 cm^{-1} for the adsorption of CO directly on the O vacancy in both rutile and anatase defective surfaces.[65] In the spectral region of frequencies lower than free CO, the spectra of CO adsorbed on the $Al/Ti/SiO_2$ material possessed two small absorption bands located at 2110 and 2095 cm^{-1}. Although these bands overlap with those we have earlier ascribed to physisorbed ^{13}CO and ^{13}CO adsorbed on OH groups, their intensity at such low CO coverage does not correspond to the natural abundance of ^{13}C. Furthermore, they were absent in the spectrum of the Al/SiO_2 sample at the same low CO coverages (Figure 5f). We therefore tentatively assign these absorption bands to unstable interaction of CO with reduced Ti^{3+} and Ti^{3+}-R species.

The impregnation of zirconocene did not lead to the generation of new absorption bands in the FT-IR spectra of CO adsorbed on the $Zr/Al/SiO_2$ and $Zr/Al/Ti/SiO_2$ catalyst materials (Figure 5g–i) as the features of these spectra are analogous to those of their corresponding precursors (Figure 5d–**f**). However, the absorption bands of moderate and weak Al^{3+} LAS at 2212 and 2198 cm^{-1} decreased in their intensity, thereby confirming the findings of the pyridine FT-IR spectroscopy analysis, where LAS concentration of both samples was found to have decreased after metallocene impregnation of the precursors. Notably, the presence of an absorption band at 2174 cm^{-1} in the spectrum of the modified catalyst (i.e., $Zr/Al/Ti/SiO_2$) is more pronounced than it was for the spectrum of the precursor

material (Figure 5f), giving more validation to the presence of O vacancy related (5-c)Ti^{4*+} sites.

Because the Ti/SiO_2 support was found to be activated toward the polymerization of ethylene by both MAO and TiBA, the investigation of surface species with CO FT-IR spectroscopy was also conducted with the SiO_2 and Ti/SiO_2 supports pre-contacted with TiBA (Figure 6).

This analysis was performed to confirm the presence, and therefore the spectral assignments of the Ti species found in the $Al_{MAO}/Ti/SiO_2$ system, specifically those related to the presence of O vacancies, which were not unequivocally visible, with the aim to further investigate the Ti species that might be responsible for the polymerization of ethylene.

The FT-IR spectra of CO adsorbed on $Al_{TiBA}+SiO_2$ (Figure 6a) shows the absorption bands of CO interacting with OH and physisorbed CO at 2158 and 2137, respectively. The bands at 2203 and 2189 cm^{-1}, ascribed to Al^{3+} species with different Lewis acid character, indicate that the Lewis acidity of TiBA is lower than that characterizing MAO. The lower acidity can be attributed to the bulkier nature of the isobutyl ligands of TiBA compared to the methyl ones of MAO. Similarly to MAO, the difference in acidity between Al species responsible for the two bands is presumably due to the different number of oxygens in the Al coordination sphere. Therefore, the absorption bands at 2203 cm^{-1} and at 2189 cm^{-1} can be ascribed to Al^{3+} moderate and weak LAS centers of the type O_2AliBu and $OAliBu_2$, respectively. Both $Al_{TiBA}+SiO_2$ and Al_{MAO}/SiO_2 sample were not active for the polymerization of olefins, so these LAS species alone cannot be responsible for catalytic activity. The same Lewis acidic Al species were generated by the interaction of TiBA with the Ti/SiO_2 support, as evident by the presence of the absorption bands at 2203 cm^{-1} and 2189 cm^{-1} (Figure 6b). The absorption band located at 2189 cm^{-1} was more intense in the Ti/SiO_2 support (Figure 6c), which might indicate a higher concentration of weak TiBA LAS. However, as this vibration overlaps with that of CO interacting with 5-coordinated Ti^{4+}, the possibility that residual (5-c)Ti^{4+} also contributed to this absorption band cannot be excluded.

Most interestingly, a clear band was visible at 2174 cm^{-1}, which therefore unequivocally identified the presence of (5-c)Ti^{4*+} as a consequence of the creation of O vacancies due to reduction by TiBA. As already mentioned, CO adsorbed on reduced TiO_2 was reported to preferentially adsorb on Ti cations located in the vicinity of an O vacancy, and not on the vacancy site itself.[55,56,62] Specifically, the next-nearest-neighbor (NNN) five-coordinate Ti atoms close to a bridge-bonded oxygen vacancy is where CO preferentially adsorbs, as also supported by DFT calculations and Scanning Tunneling Microscopy (STM) studies.[55,65,66] Combining these studies with the spectral features of the samples analyzed in this study, we can assign CO adsorbed on Ti species as indicated in Figure 7. On the TiO_2 layer of the Ti/SiO_2 material, CO adsorbs on undercoordinated Ti^{4+} surface sites, inducing a blue shift to its vibration frequency to 2185 cm^{-1} for (5-c)Ti^{4+} and to ~2210 cm^{-1} for lower coordination sites on edges.[52,53,55–57]

When a V_O is introduced on the TiO_2 surface, in this case by MAO or TiBA reduction, the excess electrons of the Ti^{3+} at the V_O are delocalized over the adjacent Ti cations.[67] CO does not adsorb on the vacancy itself (Ti^{3+}), but on the NNN (5-c)Ti^{4*+} atom, where * indicates its intermediate character between Ti^{3+} and Ti^{4+}, due to charge delocalization of the V_O. This leads to a partial occupation of the π-antibonding orbital of CO via back-bonding from the extra electron of the V_O, which weakens the carbon-oxygen. The results is a red shift in its vibration frequency of 11 cm^{-1} to 2174 cm^{-1} in respect to CO adsorbed on further (5-c)Ti^{4+} sites from the vacancy, which are unaffected by the extra electrons and which vibration is equal to that of defect-free surface Ti (2185 cm^{-1}).[55,56,62,65,66] If the concentration of vacancies were to increase to a coverage of 0.5, the charge would no longer be delocalized and CO would then preferentially adsorb on the vacancy, according to DFT calculations and STM studies, inducing a significant red shift ($\Delta\upsilon > -150$ cm^{-1}) from the free-CO vibration.[55,65,66] For this sample, no sign of CO interacting with Ti^{3+} species is visible at low coverages of CO, as evidenced by the lack of signal at frequencies lower than that of physisorbed CO. In an analogous system of TEA/$TiCl_x$/SiO_2, the adsorption of CO on reduced Ti^{3+} surface sites was also not detected, although its presence was verified by UV-Vis DR spectroscopy. This was attributed to such species not being accessible by CO due to being in clusters or to steric hindrance of the aluminum alkyls.[68] Recently, Piovano *et al.* explored the challenges to probe Ti^{3+} surface species in Ziegler-Natta

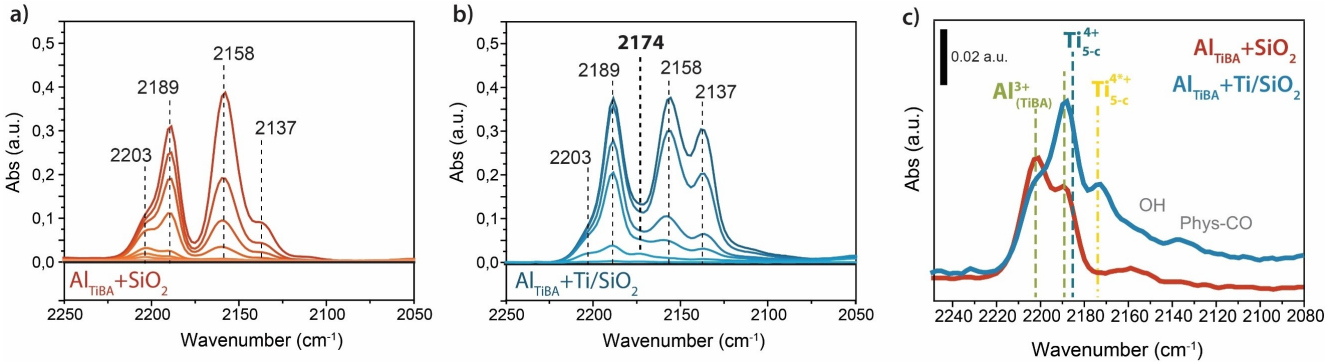

Figure 6. Fourier Transform-Infrared (FT-IR) spectra upon CO adsorption at 85 K. a) Al_{TiBA}/SiO_2 and b) Ti/SiO_2 + TiBA with increasing pressure of CO and overlap of two spectra for comparison in c). All spectra are normalized and the result of subtraction with the spectra prior CO adsorption.

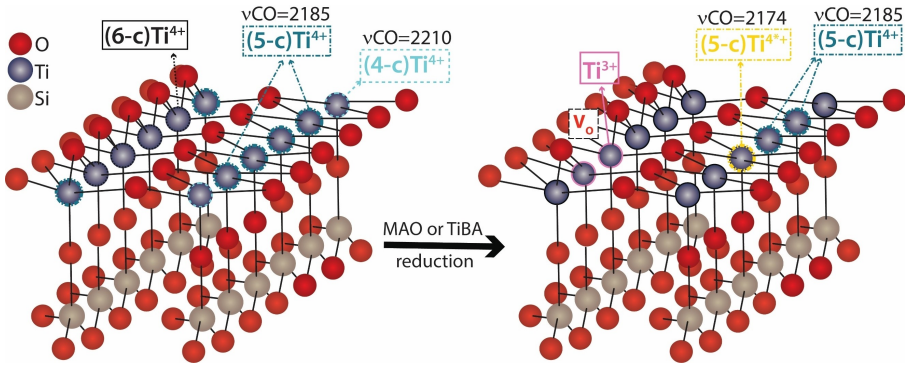

Figure 7. Ball-and-stick schematic representation of the TiO_2 layer on SiO_2 which highlights the different Ti surface species before (left) and after (right) reduction with methylaluminoxane (MAO) or tri-isobutylaluminum (TiBA). The vibration frequency of CO (in cm^{-1}) adsorbed on the Ti^{4+} species with different coordination environments are also indicated. On defect-free surfaces, CO adsorbs on undercoordinated Ti^{4+}, which leads to a blue shift of his vibration to 2185 cm^{-1} for the 5-coordinated site and to ~2210 cm^{-1} for the 4-coordinated edge sites. After reduction with MAO or TiBA, oxygen vacancies (V_O) are created. Each V_O leaves two reduced Ti^{3+} behind, which charges are delocalized, causing CO to preferentially adsorb on the next-nearest-neighbor (NNN) 5-c Ti^{4*+}atom, inducing a ~11 cm^{-1} red shift (2174 cm^{-1}) compared to the vibration of CO adsorbed on further 5-c Ti^{4+} (2185 cm^{-1}), due to the back-bonding from these delocalized charges to the antibonding orbitals of the adsorbed CO molecule.

catalyst materials with CO as probe molecule, thereby addressing the weak interaction of surface species with CO, as well as their low concentrations and sensitivity towards poisons.[63]

Hence, the lack of peaks ascribed to reduced Ti^{3+} species does not exclude their presence in the sample, as their occurrence was already addressed by the UV-Vis-DRS measurement previously mentioned (see also SI), but rather the preferential adsorption of CO to neighboring Ti^{4*+} sites.

Nonetheless, we can conclude that V_O and therefore reduced Ti species are the responsible sites for the catalytic activity of the modified Ti/SiO_2 support material. In fact, in the bare Ti/SiO_2 support, undercoordinated Ti^{4+} species were already present, but in the absence of either MAO or TiBA Al-based activators, such species were not capable of polymerizing ethylene (Table 2). Furthermore, literature findings by Barzan *et al.* on a H_2-reduced[69] and H_2-photoreduced[70] TiO_2, which were found to be active in the polymerization of ethylene, confirmed that such activity was unequivocally ascribed to Ti^{3+} species. Interestingly, because no alkylating agent was employed by Barzan *et al.*, their samples did not contain any Ti–R moieties. Hence, the reduction of the TiO_2 layer by MAO or TiBA in the modified support material creates oxygen vacancies and therefore reduced Ti^{3+} species, which are responsible for the olefin polymerization activity in the modified support materials.

Conclusion

A modified Ti/SiO_2 support for zirconocene-based ethylene polymerization catalyst materials was investigated to uncover the origin of the improved catalytic activity toward the polymerization of ethylene when compared to the corresponding non-modified SiO_2-supported catalyst system. Interestingly, this Ti/SiO_2 support was found to be capable of polymerizing ethylene by itself when in contact with an Al-based co-catalyst, such as MAO or TiBA, in the absence of any zirconocene, indicating the presence of a second (solely Ti-based) active site to the Zr centers in the modified $Zr/Al/Ti/SiO_2$ catalyst. As the polyethylene produced by the modified precursor material (i.e., $Al/Ti/SiO_2$) and the modified and commercial catalyst materials (i.e., $Zr/Al/Ti/SiO_2$ and $Zr/Al/SiO_2$, respectively) were all found to be linear, non-branched HDPE, it was concluded that these Ti active sites do not oligomerize ethylene, but polymerize it into a PE chain, indistinguishable from that produced by the Zr main active sites. Furthermore, the boost in activity for $Zr/Al/Ti/SiO_2$ was higher than the sum of the activity of the Ti and Zr active centers alone, signifying that the role of Ti was not only limited to its capability of polymerizing ethylene, but that a synergetic effect between the Ti and Zr active sites also existed. This synergetic effect was also shown in the early-stage ethylene polymerization kinetics, as observed with *in-situ* DRIFT spectroscopy, which provided new insights into the competing dynamics between these two families of active sites and hinted toward an earlier catalyst particle fragmentation of the $Zr/Al/Ti/SiO_2$ catalyst material. Probe molecule FT-IR and UV-Vis Diffuse Reflectance Spectroscopy identified that the increased ethylene polymerization activity of the Ti/SiO_2 support to be caused by its reduction by MAO or TiBA, which introduced oxygen vacancies (V_O) and the formation of reduced Ti^{3+} species in the TiO_2 layer of the modified precursor materials, which are believed to be the Ti-based active sites. Furthermore, the presence of the undercoordinated $Ti^{4+}{}_{c.u.s.}$ in the titanated support material increased the amount of Lewis acids of the $Al/Ti/SiO_2$ precursor, which lead to a more efficient activation of zirconocene (i.e., resulting in a higher concentration of Zr active sites), further contributing to the higher catalytic activity of the modified $Zr/Al/Ti/SiO_2$ catalyst material.

Experimental Section

Catalyst Synthesis

Commercial SiO_2 (ES70 W, PQ Corporation) was first dried under N_2 flow at 120 °C for 1 h to remove any physisorbed water. The temperature was then raised to 450 °C for 4 h to partially dehydroxylate the silica. Co-catalyst impregnation was performed by mixing the dry silica support to a solution of methylaluminoxane (MAO – 13 wt.% Al in toluene, Akzo-Nobel) for 4 h under reflux, while in an inert atmosphere, with the target loading of 14 wt.% Al. The Al/SiO_2 precursor so obtained was then impregnated with a toluene solution of the metallocene catalyst Cp_2ZrMe_2 (Bis(cyclopentadienyl) dimethyl-zirconium(IV) 97%, Sigma Aldrich) for 2 h at room temperature to reach the desired metallocene loading of 1.2 wt.% (0.44 Zr wt.%). After impregnation, the catalyst was filtered and rinsed with dry toluene and pentane (both anhydrous, dried over molecular sieves, Ar, ChemSeal) and then further dried under vacuum to remove remaining solvent traces.

The *Ti/SiO₂* support was obtained from the same commercial SiO_2 (ES70W, PQ Corporation), which was first dried at 120 °C for 1 h to remove any physisorbed water and then mixed with a solution of titanium alkoxide (propyl butyl titanate, Tytan™ BIP, Borica Co. Ltd.) in hexanes. The solvent was removed from the suspension by evacuation and the remaining Ti impregnated silica was thermally treated at 450 °C for 4 h under nitrogen flow, leading to a 3.5 wt. % Ti content.[27] *Al/Ti/SiO₂* and *Zr/Al/Ti/SiO₂* were obtained following the same MAO co-catalyst and metallocene impregnation procedures used for the SiO_2-supported samples, as described above.

Catalyst Testing

The olefin polymerization activity of the supported catalysts was tested in a slurry-phase Parr batch reactor, equipped with an inner quartz vial. The reactor was first loaded in N_2 atmosphere with 4 mg of catalyst material and 15 ml of heptane (n-heptane, anhydrous, over molecular sieves, Ar, ChemSeal) as a diluent, with 20 µl of tri-isobutyl aluminum (TiBA, 13.4 Al%, Sigma-Aldrich) as impurities scavenger. The closed reactor was then transferred out of the N_2-box, heated to 55 °C and pressurized with 9 bar ethylene (C_2H_4 4.0, Linde). Gas lines were flushed with N_2 and vacuum cycles before pressurization of the autoclave reactor. Reactions were stopped by depressurizing the reactor and quenched with ethanol. The obtained polyethylene-catalyst particles were then left drying at room temperature overnight to remove any solvent before weighing the polymer yield.

Catalyst characterization

Diffuse Reflectance Infrared Fourier Transform (DRIFT) spectroscopy data were collected with a Perkin Elmer Frontier instrument, equipped with a Praying Mantis™ Diffuse Reflectance Accessory (DRA) and a Mercury-Cadmium-Telluride (MCT) detector. Each experiment was performed by loading 20–22 mg of catalyst sample, in a high-temperature reaction chamber (Harrick Scientific Products Inc.) over a porous frit, equipped with gas inlets and outlets and a dome with KBr windows of 15 mm in diameter and 2 mm in thickness. The loading was done in an inert atmosphere, after which the closed cell was transferred to the spectrometer and connected to the gas lines. All lines were equipped with moisture and oxygen filters and flushed with N_2 before introducing ethylene to the catalyst chamber. Ethylene polymerization reactions were performed at 2.5 ml/min of ethylene flow and room temperature. The DRIFT spectra were collected every 20 s, in the range of 4000–1000 cm^{-1} with 4 cm^{-1} resolution, and each averaged on 8 scans. The spectra were collected, while flowing ethylene over the sample were first corrected by subtracting the spectrum of the pure catalyst material. The *in-situ* kinetic curves were obtained by summing the area of the polyethylene CH_x vibrational stretching bands and plotted over time. The first derivative of each curve was used to estimate their polymerization rates.

Fourier Transform Infrared Spectroscopy with CO and Pyridine as Probe Molecules. Self-supported wafers of 7 mm in diameter of the sample were made by pressing 4 mg of each material in a stainless-steel collar (1.5 ton – pixie hydraulic press, PIKE Technologies) and then placed inside a sealed cell under nitrogen atmosphere. This cell could sustain high vacuum and temperatures ranging from −200 °C up to 700 °C. The experimental procedure for measuring Fourier Transform Infrared (FT-IR) spectroscopy data varied depending on the probe molecule of choice. For CO as probe molecule, the closed cell containing the sample wafer was first evacuated for 30 min, then the temperature was decreased with liquid N_2 to −188 °C, at which temperature CO could chemisorb on the sample. Small amounts of CO (10% in He, 99.9% purity) were added stepwise from 0.001 mbar to 1 mbar, while taking FT-IR spectra at every set of CO pressure. FT-IR spectra were collected in the range of 1000–4000 cm^{-1} with a 4 cm^{-1} resolution, each averaged on 32 scans on a Perkin-Elmer 2000 FT-IR spectrometer with a Mercury-Cadmium-Telluride (MCT) detector. For pyridine as probe molecule, the closed cell containing the sample wafer was first evacuated for 30 min, then the sample was saturated with pyridine (20 mbar of pyridine were introduced and left in the cell chamber for 30 min at room temperature). The cell was then evacuated to remove all excess pyridine and heated with a 2.5 °C/min ramp to 423 K. The temperature was then held at 423 K for 30 min, after which the spectrum used for quantification of acid sites was collected. FT-IR spectra were collected in the range of 1000–4000 cm^{-1}, with a 4 cm^{-1} resolution, each averaged on 32 scans on a Nicolet™ iS5 FT-IR spectrometer with a Deuterated Triglycine Sulfate (DTGS) detector.

Acknowledgements

Laura de Kort (Utrecht University, UU) is acknowledged for performing the DSC measurements. Peter de Peinder (UU) and Alessandro Piovano (University of Turin) are thanked for the useful discussion on the infrared spectroscopy data interpretation. Nikolaos Nikolopoulos (UU) is thanked for the fruitful discussion and the UV-Vis-DRS measurements. Guusje Delen (UU) is thanked for the feedback on the text revision. Coen Mulder and Helen de Waard (UU) are acknowledged for performing the ICP-OES experiments. The authors acknowledge project funding from TotalEnergies.

Conflict of Interest

The authors declare no conflict of interest.

Data Availability Statement

The data that support the findings of this study are available from the corresponding author upon reasonable request.

Keywords: polymerization · metallocene · catalyst · titania · IR spectroscopy

[1] G. G. Hlatky, *Coord. Chem. Rev.* **1999**, *181*, 243–296.
[2] E. O. Fischer, W. Pfab, *Z. Naturforsch. B* **1952**, *7*, 377–379.
[3] G. Wilkinson, J. M. Birmingham, *J. Am. Chem. Soc.* **1954**, *76*, 4281–4284.
[4] H. Sinn, W. Kaminsky, H.-J. Vollmer, R. Woldt, *Angew. Chem. Int. Ed. Engl.* **1980**, *19*, 390–392.
[5] W. Kaminsky, *Metalorganic Catalysts for Synthesis and Polymerization*, Springer, Berlin, **1999**.
[6] W. Kaminsky, *Macromolecules* **2012**, *45*, 3289–3297.
[7] P. Cossee, *J. Catal.* **1964**, *3*, 80–88.
[8] W. Kaminsky, *J. Chem. Soc. Dalton Trans.* **1998**, 1413–1418.
[9] T. K. Trefz, M. A. Henderson, M. Linnolahti, S. Collins, J. S. McIndoe, *Chem. Eur. J.* **2015**, *21*, 2980–2991.
[10] H. S. Zijlstra, S. Harder, *Eur. J. Inorg. Chem.* **2015**, *2015*, 19–43.
[11] M. E. Z. Velthoen, J. M. Boereboom, R. E. Bulo, B. M. Weckhuysen, *Catal. Today* **2019**, *334*, 223–230.
[12] S. Collins, M. Linnolahti, M. G. Zamora, H. S. Zijlstra, M. T. Rodríguez Hernández, O. Perez-Camacho, *Macromolecules* **2017**, *50*, 8871–8884.
[13] E. P. Talsi, N. V. Semikolenova, V. N. Panchenko, A. P. Sobolev, D. E. Babushkin, A. A. Shubin, V. A. Zakharov, *J. Mol. Catal. A* **1999**, *139*, 131–137.
[14] M. E. Z. Velthoen, A. Muñoz-Murillo, A. Bouhmadi, M. Cecius, S. Diefenbach, B. M. Weckhuysen, *Macromolecules* **2018**, *51*, 343–355.
[15] E. Aitola, Tailoring Polyolefin Properties by Metallocene Catalysis, University of Helsinky, Finland, **2006**.
[16] F. Ciardelli, A. Altomare, M. Michelotti, *Catal. Today* **1998**, *41*, 149–157.
[17] J. R. Severn, J. C. Chadwick, R. Duchateau, N. Friederichs, *Chem. Rev.* **2005**, *105*, 4073–4147.
[18] M. N. Cardoso, A. G. Fisch, *Ind. Eng. Chem. Res.* **2016**, *55*, 9426–9432.
[19] E. J. Choi, Seung Won; Joo, *Fouling Prediction Method in Polyolefin Production Process*, **2019**, EP003786197 A1.
[20] P. Aaltonen, B. Löfgren, *Macromolecules* **1995**, *28*, 5353–5357.
[21] G. G. Hlatky, *Chem. Rev.* **2000**, *100*, 1347–1376.
[22] J. R. Severn, J. C. Chadwick, *Tailor-Made Polymers*, Wiley, Weinheim, **2008**.
[23] J. R. Severn, J. C. Chadwick, *Dalton Trans.* **2013**, *42*, 8979–8987.
[24] J. B. P. Soares, T. F. L. McKenna, *Polyolefin Reaction Engineering*, Wiley-VCH, Weinheim, **2012**.
[25] V. F. Tisse, F. Prades, R. Briquel, C. Boisson, T. F. L. McKenna, *Macromol. Chem. Phys.* **2010**, *211*, 91–102.
[26] C. Willocq, A. Vantomme, M. Slawinski, *Modified Catalyst Supports*, **2019**, US10618987B2.
[27] C. Willocq, A. Vantomme, M. Slawinski, *Modified Catalyst Supports*, **2016**, EP2588501B1.
[28] C. Willocq, A. Vantomme, M. Slawinski, *Modified Catalyst Support*, **2011**, EP2542594B1.
[29] G. Debras, J.-P. Dath, *Titanated Chromium-Based Catalysts to Produce Polyethylene*, **1998**, EP0882743 A1.
[30] D. Cicmil, J. Meeuwissen, A. Vantomme, J. Wang, I. K. van Ravenhorst, H. E. van der Bij, A. Muñoz-Murillo, B. M. Weckhuysen, *Angew. Chem. Int. Ed.* **2015**, *54*, 13073–13079; *Angew. Chem.* **2015**, *127*, 13265–13271.
[31] T. J. Pullukat, R. E. Hoff, *Catal. Rev.* **1999**, *41*, 389–428.
[32] E. Groppo, K. Seenivasan, E. Gallo, A. Sommazzi, C. Lamberti, S. Bordiga, *ACS Catal.* **2015**, *5*, 5586–5595.
[33] B. Jongsomjit, S. Ngamposri, P. Praserthdam, *Catal. Lett.* **2005**, *100*, 139–146.
[34] B. Jongsomjit, S. Ngamposri, P. Praserthdam, *Molecules* **2005**, *10*, 672–678.
[35] A. G. Fisch, N. S. M. Cardozo, A. R. Secchi, F. C. Stedile, P. R. Livotto, D. S. de Sá, Z. N. da Rocha, J. H. Z. dos Santos, *Appl. Catal. A* **2009**, *354*, 88–101.
[36] S. Zanoni, N. Nikolopoulos, A. Welle, V. Cirriez, B. M. Weckhuysen, *ChemCatChem* **2023**, *15*, e202300222.
[37] J. P. Gallas, J. M. Goupil, A. Vimont, J. C. Lavalley, B. Gil, J. P. Gilson, O. Miserque, *Langmuir* **2009**, *25*, 5825–5834.
[38] J. P. Gallas, J. C. Lavalley, A. Burneau, O. Barres, *Langmuir* **1991**, *7*, 1235–1240.
[39] K. Hadjiivanov, in *Adv. Catal.*, Academic Press Inc., Sofia, **2014**, pp. 99–318.
[40] A. Davydov, *Molecular Spectroscopy of Oxide Catalyst Surfaces*, Wiley, Chichester, **2003**.
[41] Z. Buniazet, J. Couble, D. Bianchi, M. Rivallan, A. Cabiac, S. Maury, S. Loridant, *J. Catal.* **2017**, *348*, 125–134.
[42] X. Gao, I.E. Wachs, *Catal. Today* **1999**, *51*, 233–254.
[43] V. N. Panchenko, N. V. V. Semikolenova, I. G. G. Danilova, E. A. A. Paukshtis, V. A. A. Zakharov, *J. Mol. Catal. A* **1999**, *142*, 27–37.
[44] M. Low, A. Severdia, J. Chan, *J. Catal.* **1981**, *69*, 384.
[45] M. A. Bashir, T. Vancompernolle, R. M. Gauvin, L. Delevoye, N. Merle, V. Monteil, M. Taoufik, T. F. L. L. McKenna, C. Boisson, *Catal. Sci. Technol.* **2016**, *6*, 2962–2974.
[46] D. Bianchini, J. H. Z. dos Santos, T. Uozumi, T. Sano, *J. Mol. Catal. A* **2002**, *185*, 223–235.
[47] G. Fink, B. Steinmetz, J. Zechlin, C. Przybyla, B. Tesche, *Chem. Rev.* **2000**, *100*, 1377–1390.
[48] T. Kataoka, J. A. Dumesic, *J. Catal.* **1988**, *112*, 66–79.
[49] S. M. Jung, P. Grange, *Appl. Catal. A* **2002**, *228*, 65–73.
[50] G. Pérez-López, R. Ramírez-López, T. Viveros, *Catal. Today* **2018**, *305*, 182–191.
[51] M. Khalifa, M. Hajji, H. Ezzaouia, *EPJ Web Conf.* **2012**, *29*, 00014.
[52] L. Mino, A. M. Ferrari, V. Lacivita, G. Spoto, S. Bordiga, A. Zecchina, *J. Phys. Chem. C* **2011**, *115*, 7694–7700.
[53] L. Mino, G. Spoto, S. Bordiga, A. Zecchina, *J. Phys. Chem. C* **2012**, *116*, 17008–17018.
[54] Z. Buniazet, J. Couble, D. Bianchi, M. Rivallan, A. Cabiac, S. Maury, S. Loridant, *J. Catal.* **2017**, *348*, 125–134.
[55] M. Xu, H. Noei, K. Fink, M. Muhler, Y. Wang, C. Wöll, *Angew. Chem. Int. Ed.* **2012**, *51*, 4731–4734; *Angew. Chem.* **2012**, *124*, 4810–4813.
[56] M. Xu, Y. Cao, R. Xu, S. Hu, S. Yan, *Phys. Chem. Chem. Phys.* **2014**, *16*, 23711–23715.
[57] C. Rohmann, Y. Wang, M. Muhler, J. Metson, H. Idriss, C. Wöll, *Chem. Phys. Lett.* **2008**, *460*, 10–12.
[58] K. Hadjiivanov, B. M. Reddy, H. Knözinger, *Appl. Catal. A* **1999**, *188*, 355–360.
[59] K. Hadjiivanov, A. Penkova, M. A. Centeno, *Catal. Commun.* **2007**, *8*, 1715–1718.
[60] S. Jayashree, M. Ashokkumar, *Catalysts* **2018**, *8*, 601.
[61] X. Chen, L. Liu, P. Y. Yu, S. S. Mao, *Science* **2011**, *331*, 746–750.
[62] H. Noei, L. Jin, H. Qiu, M. Xu, Y. Gao, J. Zhao, M. Kauer, C. Wöll, M. Muhler, Y. Wang, *Phys. Status Solidi* **2013**, *250*, 1204–1221.
[63] A. Piovano, J. Zarupski, E. Groppo, *J. Phys. Chem. Lett.* **2020**, *11*, 5632–5637.
[64] P. Pletcher, A. Welle, A. Vantomme, B. M. Weckhuysen, *J. Catal.* **2018**, *363*, 128–135.
[65] P. G. Lustemberg, D. A. Scherlis, *J. Chem. Phys.* **2013**, *138*, 124702.
[66] Y. Zhao, Z. Wang, X. Cui, T. Huang, B. Wang, Y. Luo, J. Yang, J. Hou, *J. Am. Chem. Soc.* **2009**, *131*, 7958–7959.
[67] T. Minato, Y. Sainoo, Y. Kim, H. S. Kato, K. Aika, M. Kawai, J. Zhao, H. Petek, T. Huang, W. He, B. Wang, Z. Wang, Y. Zhao, J. Yang, J. G. Hou, *J. Chem. Phys.* **2009**, *130*, 124502.
[68] A. Piovano, G. A. Martino, C. Barzan, *Rend. Lincei* **2017**, *28*, 43–49.
[69] C. Barzan, E. Groppo, S. Bordiga, A. Zecchina, *ACS Catal.* **2014**, *4*, 986–989.
[70] C. Barzan, L. Mino, E. Morra, E. Groppo, M. Chiesa, G. Spoto, *ChemCatChem* **2017**, *9*, 4324–4327.
[71] N. I. Mäkelä, H. R. Knuuttila, M. Linnolahti, T. A. Pakkanen, M. A. Leskelä, *Macromolecules* **2002**, *35*, 3395–3401.
[72] D. Coevoet, H. Cramail, A. Deffieux, *Macromol. Chem. Phys.* **1998**, *199*, 1459–1464.
[73] V. N. Panchenko, V. A. Zakharov, E. A. Paukshtis, *J. Mol. Catal. A* **2005**, *240*, 33–39.
[74] A. Muller, E. Diemann, C. K. Jorgensen, in *Struct. Bond.*, Springer-Verlag, Berlin, **1973**, pp. 23–48.
[75] C. K. Jorgensen, in *Struct. Bond.*, Springer-Verlag, Berlin, **1966**, pp. 234–248.
[76] J. A. Duffy, in *Struct. Bond. Vol 32*, Springer-Verlag, Berlin, **1977**, pp. 147–166.
[77] J. M. Fraile, J. I. Garcia, J. I. Mayoral, E. Vispe, *J. Catal.* **2005**, *233*, 90–99.

Manuscript received: February 8, 2023
Revised manuscript received: March 18, 2023
Accepted manuscript online: March 29, 2023
Version of record online: May 3, 2023